

# **JGR Space Physics**

### RESEARCH ARTICLE

10.1029/2023JA031595

#### **Key Points:**

- Over 60% of the microinjection satisfy the drift mirror instability (DMI) criteria, emphasizing the importance of the DMI as one of the generation
- Diamagnetic cavities can be the origin for the observed DMI events
- The sources of the electron population of non-DMI microinjection have strong association with the inward, Parker Spiral interplanetary magnetic field and require further study

#### **Supporting Information:**

Supporting Information may be found in the online version of this article.

#### Correspondence to:

Y.-L. Liou, liouy@my.erau.edu

#### Citation:

Liou, Y.-L., Nykyri, K., Kavosi, S., & Ma, X. (2023). Statistical study of the energetic electron microinjections at the high-latitude magnetosphere. *Journal of Geophysical Research: Space Physics*, 128, e2023JA031595. https://doi.org/10.1029/2023JA031595

Received 14 APR 2023 Accepted 26 SEP 2023

# © 2023. American Geophysical Union. All Rights Reserved.

# Statistical Study of the Energetic Electron Microinjections at the High-Latitude Magnetosphere

Yu-Lun Liou<sup>1</sup>, Katariina Nykyri<sup>1</sup>, Shiva Kavosi<sup>1</sup>, and Xuanye Ma<sup>1</sup>

<sup>1</sup>Embry-Riddle Aeronautical University, Daytona Beach, FL, USA

**Abstract** Understanding the formation of the seed population for the energetic electrons trapped within the Earth's Van Allen radiation belts has been under debate for decades. The magnetic reconnection in the Earth's magnetotail during the substorms is the main process of accelerating the electrons to the tens to hundreds of keV. These electrons are further injected toward the radiation belts, where they get further accelerated to relativistic energies. Recently, it has been suggested that another source could come from the dayside diamagnetic cavities where electrons and ions can be locally energized to hundreds of keV energies. It has been shown that the physical mechanism within the cavities can create a strong acceleration perpendicular to magnetic field, which can lead to temperature anisotropy and drift mirror instability. The electron fluxes localized within the troughs of the mirror mode waves exhibit the counter-streaming "microinjection" signature. To investigate the origin of microinjections and their dependence on solar wind conditions, here we have performed an event search and a statistical study of their properties encompassing a total of ~165 hr (47 microinjection events) of Magnetospheric Multiscale observations at the pre-dusk sector high-latitude boundary layer. The ultralow frequency range magnetic field fluctuations coincided with the counter-streaming energetic electron fluxes. For most events, the interplanetary magnetic field was duskward and anti-sunward; over 60% of these microinjections satisfy the criteria of the drift mirror instability, which indicates the temperature anisotropy could play an important role for the microinjection.

Plain Language Summary Studying the source and acceleration mechanisms of the high-energy particles is crucial for understanding the radiation environment in the near-Earth space. The Van Allen radiation belts, with the shape of donuts around the Earth from an altitude of  $0.2-2 R_F$  (inner belts) and  $3-8 R_F$  (outer belt), are formed by trapped energetic particles. Several mechanisms are proposed as seed population for the radiation belt electrons which can be then accelerated to relativistic energies. Recently dayside structures at the high-latitude magnetosphere called diamagnetic cavities are suggested to be one of the possible sources both for the high-energy particles (ten to hundreds of keV) and the temperature anisotropy to the magnetosphere. A recent Magnetospheric Multiscale observation has shown that the electron fluxes (>100 keV) are modulated by the mirror mode waves at the high-latitude magnetosphere, exhibiting a counter-streaming (particles flow simultaneously parallel and anti-parallel to magnetic field signature, called "microinjection"). The waves which are created by the drift mirror instability locally require a strong temperature anisotropy. It makes the diamagnetic cavity to be one of the candidates for the generation of the microinjection. As the location of those cavities are strongly dependent on the interplanetary magnetic field (IMF) orientation, studying on the interaction between the IMF and magnetosphere could help further realize the possible source for the periodic electron fluxes. With this intent, 47 microinjection events are presented in this article. We examined the relation between the electron fluxes and the IMF orientation together with the analysis of the drift mirror instability. We show that the temperature anisotropy plays an important role for the formation of the microinjection.

#### 1. Introduction

The charged particles injected into the Earth's inner magnetosphere could become the seed for relativistic and ultra-relativistic electrons. These energetic electrons, generally from ten to several hundred keV, have been observed near the geosynchronous orbit and reported as substorm-associated processes by Arnoldy and Chan (1969). During the substorm onset, the seed population originating from the near-Earth plasma sheet is accelerated by the tail reconnection related processes and is rapidly transported toward the Earth's radiation belts (Turner et al., 2017).

LIOU ET AL.



More localized scale injections have been measured in the inner magnetosphere and are called microinjections (Sarafopoulos, 2002). As a new type of injection, the microinjection events typically present repetitive characteristics of fluxes in the ultralow frequency (ULF) range, commonly corresponding to ~5 min period. From the Interball/DOK-2 instrument, it was suggested that a meandering isospectrum surface probably explains the formation of the dispersive (higher energy electrons arrive sooner to the observation region) microinjections (Sarafopoulos, 2002). More recently, the dispersive properties of the microinjections, detected by the Magnetospheric Multiscale (MMS) mission, were analyzed (Fennell et al., 2016). The energetic electrons were tracked back to their origin along the drift path and showed that the source regions of the fluxes were approximately close to the flank of the magnetopause. Additionally, by the aims of the MMS and OpenGGCM simulations, Kavosi et al. (2018) explored several potential processes near the magnetopause and proposed that the Kelvin-Helmholtz instabilities (KHI) and flux transfer events (FTEs) are associated with triggering the energetic electron microinjections.

The dispersive signature of the electron injections in the above studies is strongly indicative of the acceleration and source region remote from their observation site (Fennell et al., 2016; Kavosi et al., 2018). The recent MMS observations detected microinjections without the dispersive signature, such that both low and high energies were detected simultaneously (Nykyri et al., 2021). A possible local mechanism for the microinjections could be the drift mirror instability (Nykyri et al., 2021), driven by temperature anisotropy in high-beta plasma (Hasegawa, 1969a; Pokhotelov et al., 2001).

Considering that the growth of mirror modes requires a sufficient temperature anisotropy, the instability is typically more active in the dayside magnetosheath (Hubert et al., 1989; Tsurutani et al., 1982) or the crossing of the quasi-perpendicular bow shock (Czaykowska et al., 1998, 2001; Lacombe et al., 1992). It is interesting that mirror instability can be occasionally observed inside the magnetosphere when certain mechanisms suddenly enhance the temperature anisotropy (Haerendel, 2000; Hasegawa, 1969b; Woch et al., 1988). It has been suggested that a potential source for the perpendicular temperature enhancement in the high-latitude boundary layer could possibly come from the diamagnetic cavities (DMCs) (Nykyri et al., 2019, 2021). The DMCs are the weak magnetic field, and high plasma beta regions that commonly surround the high-altitude cusp funnel, and are created by magnetic reconnection (Burkholder et al., 2021a; Nykyri, Otto, Adamson, Dougal, & Mumme, 2011; Nykyri et al., 2019). The observations within the cavities have detected particle populations up to hundreds of keV (Niehof et al., 2008; Nykyri, Otto, Adamson, Dougal, & Mumme, 2011; Nykyri et al., 2012; Walsh et al., 2010). While the ULF wave turbulence (Chen & Fritz, 1998) has been suggested as one mechanism to energize the particles in the cavities, it has been shown that the compressive fluctuations in the DMCs are mostly not waves, but can be produced by the motion of the DMC, associated boundaries and FTEs (Nykyri, Otto, Adamson, & Tjulin, 2011). Furthermore, it has been argued that the ion scale waves (Nykyri et al., 2003) do not have sufficient energy to explain the hundreds of keV energy increase in the high-altitude cusp (Nykyri et al., 2004).

Since the cavities were mainly formed by the magnetic reconnection between the solar wind and the geomagnetic fields, the locations of the DMCs can be predicted based on the interplanetary magnetic field (IMF) orientations (Nykyri et al., 2019). For the purpose of understanding the mechanism and the origin of the repetitive high-energy particle fluxes, we have performed a search of microinjections in the MMS data between 2015 and 2017. Interestingly, all of the identified ~165 hr of microinjections were detected at the dusk-sector, high-latitude magnetosphere, where the cavities can possibly form nearby or be magnetically connected to the cavity at the opposite hemisphere. Using SW and IMF data from the virtual OMNI observatory at bow shock nose (King & Papitashvili, 2005) and MMS in situ observations, we have statistically determined the relation between the ULF fluctuations, local plasma parameters, as well as the solar wind and IMF conditions to test and eliminate the possible source mechanisms for microinjections and energetic particles within them.

# 2. Instrumentation and Data Analyses

The MMS mission contains four spacecraft that are spatially separated around 10–100 km in the form of a tetrahedron. All spacecraft were equipped with identical in situ instruments for measuring magnetospheric environment. The Energetic Particle Detector (EPD) (Mauk et al., 2016) is one of the instruments onboard MMS dedicated to energetic particle investigations. Through the two sensors on the EPD: the Fly's Eye Energetic Particle Sensor (FEEPS) and Energetic Ion Spectrometer, it provides all-sky measurements for 25–650 keV electrons and 45–650 keV ions. In this paper, we focus on the high-energy electron study by the FEEPS observations.

LIOU ET AL. 2 of 11

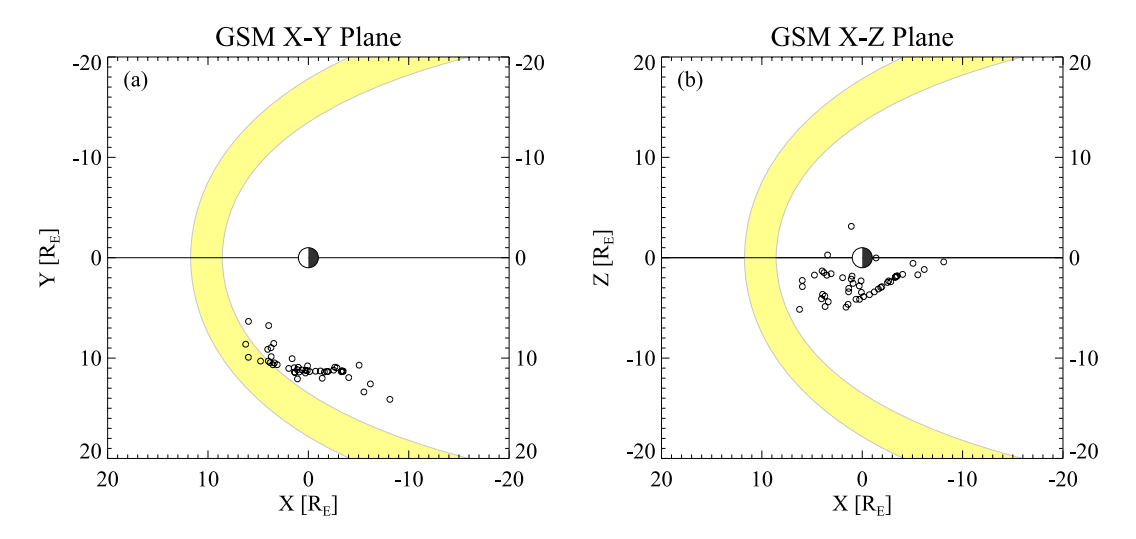


**Figure 1.** The location of Magnetospheric Multiscale 1 spacecraft in GSM coordinates. The yellow-shaded color displays the region of magnetopause under the maximum and minimum dynamic pressure during the whole observation period. The gray curves represent the magnetopause calculated by Shue et al. (1997).

The magnetic field in the magnetosphere was taken by the Fluxgate Magnetometer (FGM) (Russell et al., 2016; Torbert et al., 2016), using 8 Hz sampling rate survey data. With the combination of both FEEPS and FGM observations from the MMS spacecraft 1 (MMS1), we selected 47 intervals from the years 2015–2017 and recognized total 165 hr of microinjection activities (see Table S1 in Supporting Information S1). The plasma moments for testing the drift mirror instability condition come from Fast Plasma Investigation (FPI) (Pollock et al., 2016).

Figure 1 shows the location of the MMS1 and the shape of the magnetopause on the GSM X-Y and X-Z plane. The magnetopause between these 47 intervals is determined by an empirical model under the assumption of cylindrical symmetry on the dayside (Shue et al., 1997). During all of the intervals, the locations of MMS were inside the magnetosphere and mostly in the southern hemisphere, around both sunward ( $X_{GSM} > 0$ ) and tailward ( $X_{GSM} < 0$ ) of the dawn-dusk terminator. The bias of the spatial distribution may be due to the orbit of MMS1 during 2015–2017 (see Figure S1 in Supporting Information S1). We found that MMS1 located in the southern hemisphere over two-thirds of the time we had surveyed and spent 55% of the time in the dusk sector (see Table S2 in Supporting Information S1). This bias could possibly affect the spatial distribution of our microinjection events. However, this percentage alone could not adequately explain why the microinjections are observed exclusively in the dusk sector. We will need more observations to verify.

The upstream, near-Earth solar wind magnetic fields and dynamic pressure are provided by the High-Resolution OMNI virtual observatory (HRO) (King & Papitashvili, 2005). By integrating the spacecraft observations (ACE, Wind, IMP 8 etc.) with the techniques of time-shifting to the Earth's bow shock nose, the OMNI data sets are produced for the purposes of studying solar wind-magnetosphere interactions. Since the OMNI data set was built to reconstruct the solar wind observations at  $\sim 14~R_E$ , the propagation time of the plasma structure from the Earth's bow shock toward the magnetosphere should be taken into consideration. One can estimate a  $\sim 1.1$  min propagation time by taking the average solar wind speed 400 km/s and the location of magnetopause  $\sim 10~R_E$ . In this paper, the 5-min HRO data are used to reduce the uncertainty during the propagation. Figure 2 shows an example of the microinjection activity on the 2 August 2015. The red horizontal lines on Figure 2a label the time subintervals that were analyzed and which were clearly recognized in the frequency belt on the spectrogram (see Figure 3). The two black horizontal dash lines on Figure 3c respectively specify the pitch angles at 30° and 150°. The counter-streaming electron fluxes on Figure 3d were calculated by the summation of electron flux in  $< 30^\circ$  and  $> 150^\circ$  pitch-angle distribution.

Figures 2a and 2c demonstrate that the ULF fluctuations in magnetic field were observed simultaneously with the enhanced fluxes of counter-streaming electrons. By applying the wavelet analysis on both the FGM magnetic field and the FEEPS electron data, the periodicity spectrograms can be calculated, as depicted in Figure 3. We found that the periodicity of ULF fluctuations in the example subinterval was identified to be 400–450 s. Note

LIOU ET AL. 3 of 11

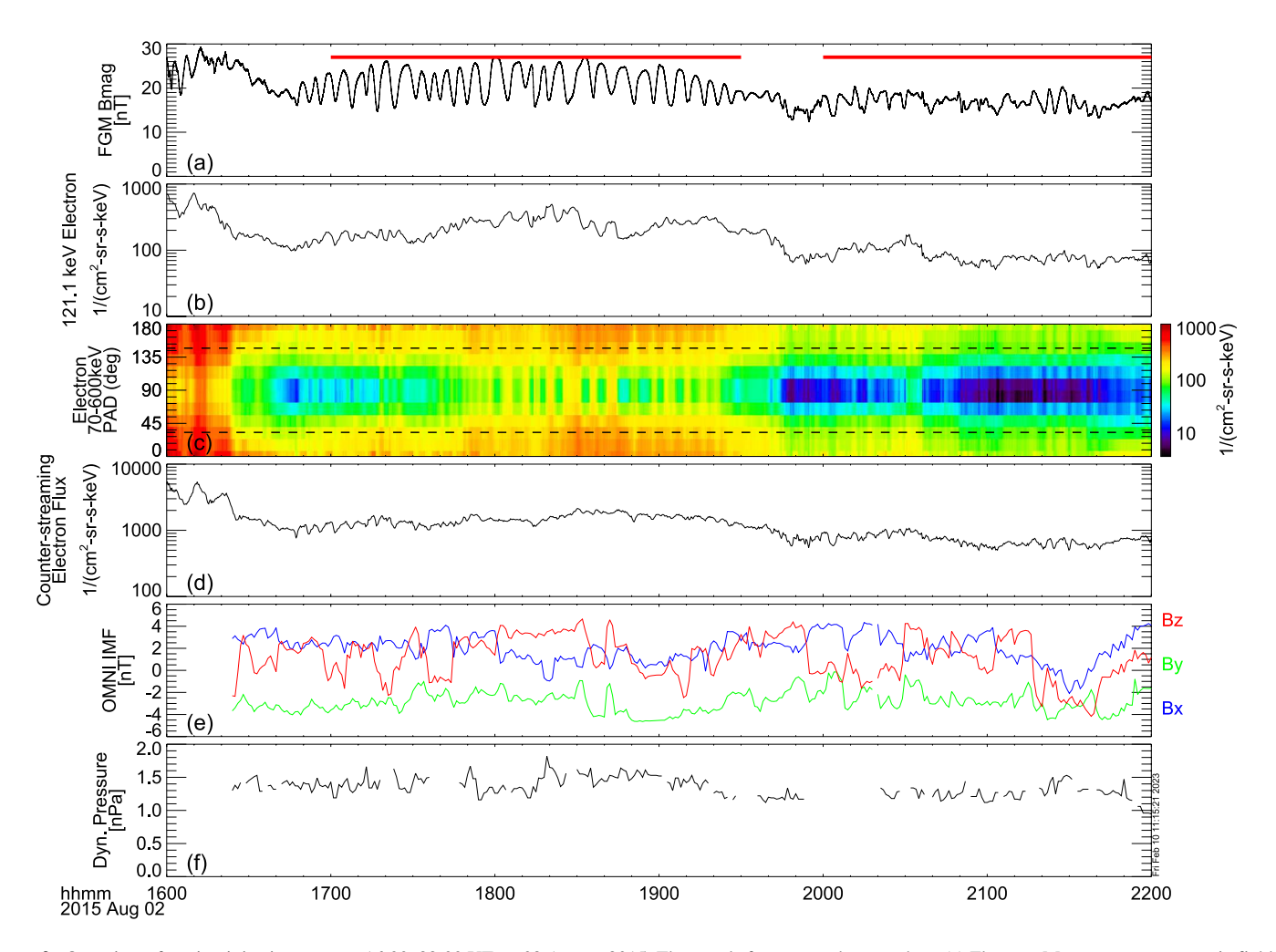


Figure 2. Overview of a microinjection event at 16:00–22:00 UT on 02 August 2015. The panels from top to bottom show (a) Fluxgate Magnetometer magnetic field strength, (b) Fly's Eye Energetic Particle Sensor omni-directional electron intensity, (c) electron pitch-angle distribution, (d) counter-streaming electron flux, (e) OMNI interplanetary magnetic field vector, and (f) solar wind dynamic pressure. The red horizontal lines on the very top panel remark the time intervals of analysis.

that the gap below 40-s period in Figure 3 occurred due to the equivalently  $\sim$ 20 s time resolution of the FEEPS 121 keV electron flux compared to FGM 0.125 s time resolution.

# 3. Statistical Results

The periodicity of the electron flux fluctuations was sorted according to the IMF clock angle and the Parker Spiral (PS) angle. The IMF clock angle  $\theta_{cl}$  is defined as the angle between the geomagnetic Z-component and the projection onto the Y-Z plane in the GSM coordinates,  $\theta_{cl} = \tan^{-1}(B_Y/B_Z)$ . The PS angle  $\theta_{ps}$  refers to the angle between the projection of IMF onto the GSM X-Y plane and the Sun-Earth direction,  $\theta_{ns} = \tan^{-1}(B_Y/B_X)$ .

For examining the drift mirror instability (DMI) during the microinjection, we introduce two linear onset criteria by Hasegawa (1969a) and Pokhotelov et al. (2001).

$$\beta_{\perp}(p_{\perp}/p_{\parallel}-1) > 1, \tag{1}$$

$$\beta_{\perp}(p_{\perp}/p_{\parallel} - 1) - \frac{k_{\parallel}^2}{k_{\perp}^2} \left( 1 + \frac{\beta_{\perp} - \beta_{\parallel}}{2} \right) > 1,$$
(2)

where  $p_{\perp}$ ,  $p_{\parallel}$  are perpendicular and parallel plasma thermal pressure,  $\beta_{\perp}$  is the ratio of plasma perpendicular thermal pressure to magnetic plasma,  $\beta_{\parallel}$  is the ratio of plasma parallel thermal pressure to magnetic plasma,  $k_{\perp}$  and

LIOU ET AL. 4 of 11

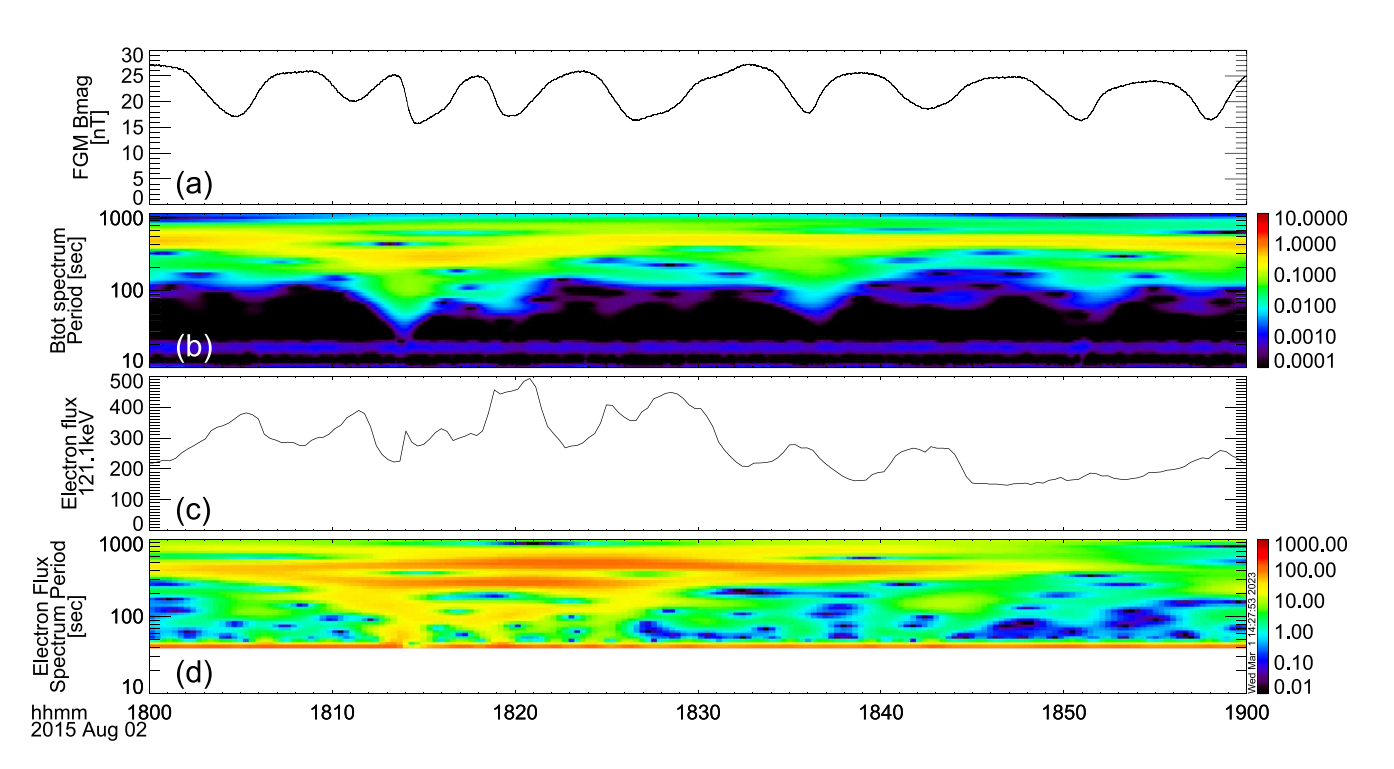


Figure 3. The time variations of (a) total magnetic field strength measured by Fluxgate Magnetometer and (c) the electron flux in 121.1 keV measured by Fly's Eye Energetic Particle Sensor during the occurring time of microinjection. The periodicity spectrograms of (b) the magnetic field magnitude and (d) the electron flux are both calculated by the wavelet analysis.

 $k_{\parallel}$  are the wave number perpendicular and parallel to the magnetic field. As the criteria by Hasegawa (1969a) in Equation 1 erroneously omitted the effect of the magnetic gradient drift which may not be neglected in our case, we applied an alternative form derived by Pokhotelov et al. (2001) (Equation 2) for checking the instability criteria. The ratio of  $k_{\parallel}^2$  to  $k_{\perp}^2$  in Equation 2 is taken from Treumann et al. (2004). While the left-hand side of these two criteria can yield slightly different values, the time intervals determined as DMI are identical for our event list. No matter which criteria is applied in our cases, the statistical results are the same. Figure 5 shows an example of the threshold value calculated by the two different forms of instability criteria. The decreased criteria values but exactly identical DMI time intervals, when including the magnetic gradient, would imply that the effect would not be sufficient to stabilize the system.

The three panels of Figure 6 present the occurrence rate distribution of the microinjections, sorted with their corresponding solar wind clock angle and periodicity. Each bin of Figure 6 has 45° azimuthally in width and 100 s radially in height. As a function of different clock angles, the oscillation period of microinjection varies from 200 to 700 s. Besides, both northward and southward IMF was observed during the overall microinjection observation time.

The DMI criteria in Equation 1 and Equation 2 are applied to identify the events that were unstable to mirror modes. The microinjections with and without satisfying the mirror mode criteria are categorized in Figures 6b and 6c. In Figure 6b, approximately 38% total occurring time of microinjection do not reach the threshold for the drift mirror instability (which are called non-DMI time hereafter). Among this activity, there are over 73% of non-DMI time is corresponding to the positive  $B_{\gamma}$  IMF component. For a more thorough understanding of the physical drivers, we also compare the pattern of the IMF PS angle as discussed later. As shown in Figure 6c on the other hand, there are over 62% of total microinjection time satisfying the drift mirror instability criteria (called DMI time hereafter). It suggests that the microinjections are more frequently observed when the ambient plasma is unstable for the mirror modes. The clock angle of the DMI microinjection demonstrates that the IMF orientations point toward dawnside (-Y) or duskside (+Y), and the direction can independently be either northward (+Z) and southward (-Z) regardless of the Y component.

Magnetic reconnection in the vicinity of the high-altitude cusp regions for the northward (southward) IMF is expected to form DMCs on the tailward (sunward) side of the high-altitude cusp (Nykyri, Otto, Adamson, Dougal, & Mumme, 2011; Nykyri et al., 2019). On the other hand, the strength and polarity of the IMF  $B_{\gamma}$ 

LIOU ET AL. 5 of 11

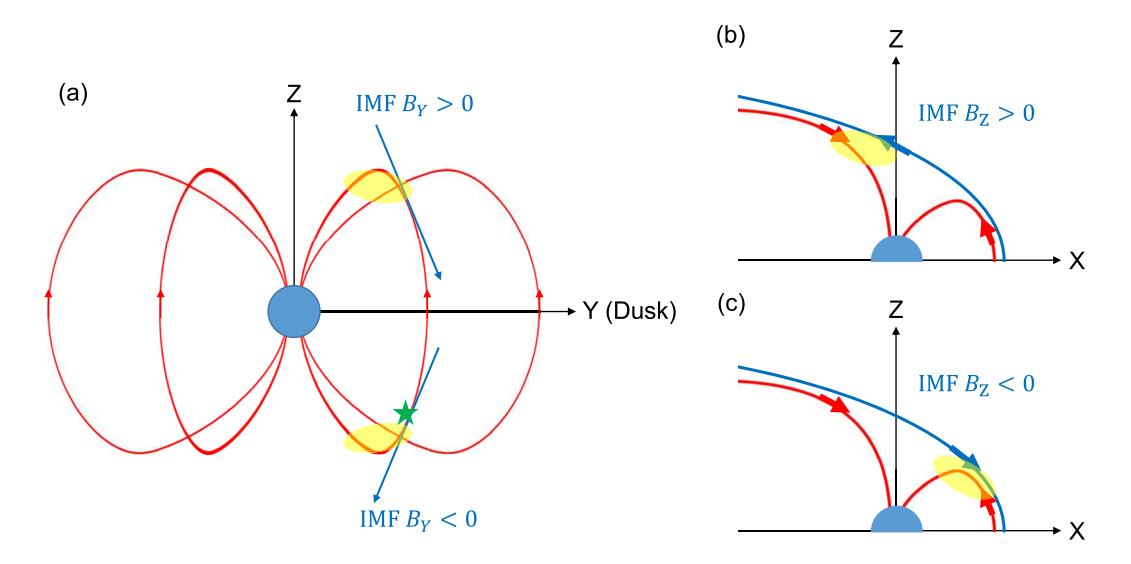


**Figure 4.** The illustration of the approximate diamagnetic cavity (DMC) location with respect to interplanetary magnetic field (IMF) orientation. The red lines are Earth's magnetic field lines, the blue lines are the IMF. The yellow shaded regions are the DMC formed by magnetic reconnection due to the antiparallel IMF. The green star in panel (a) represents the microinjection events observed at the duskside, southern hemisphere. (b) The northward IMF can create DMC at the tailward magnetosphere. (c) The southward IMF can create DMC at the sunward magnetosphere. Panel (b, c) are reproduced from Nykyri, Otto, Adamson, Dougal, and Mumme (2011). Please note that also low-latitude, component reconnection during southward and duskward (dawnward) IMF can create DMC at southern-hemispheric dusk (dawn) sector (Nykyri et al., 2019).

component determined whether the cavity can form dawn or duskward of the high-altitude cusp funnel at northern and southern hemisphere (Nykyri, Otto, Adamson, Dougal, & Mumme, 2011; Nykyri et al., 2019). As can be seen in Figure 1, the locations where MMS detected microinjections are distributed from sunward to tailward of the dawn-dusk terminator and are mostly at the southern hemisphere. If the energetic electrons were coming from the DMCs at the opposite hemisphere, the microinjection should be observed at the same field lines magnetically mapping to the location of the cavities. In other word, we expect the DMCs responsible for the DMI microinjection would locate at the duskside magnetosphere of both northward or southern hemispheres. The corresponding IMF orientations that generate the DMCs at the southern (northern) hemisphere require  $-B_v$  ( $+B_v$ ) component, as illustrating in Figure 4a. The  $+B_7$  ( $-B_7$ ) component, on the other hand, determines the location of the cavities near the tailward (sunward) of the cusp funnel (Figures 4b and 4c). In our cases, the directions of the IMF in the Y-Z plane (Figure 6c) display  $(-B_y, +B_z)$ ,  $(+B_y, +B_z)$ ,  $(+B_y, -B_z)$  and  $(-B_y, -B_z)$ . Under such these solar wind condition, the expected locations of the DMCs are respectively (southern, tailward), (northern, tailwad), (northern, sunward), and (southern, sunward). Additionally, the  $(+B_{\gamma}, -B_{\gamma})$  IMF can also generate the DMC at southern hemisphere of sunward magnetosphere. These expected locations of the diamagnetic can be responsible for accelerating the electron fluxes at the duskside high-latitude magnetosphere. The results support the case study of Nykyri et al. (2021) and indicate that the DMCs may be the source of energetic electrons observed in the microinjections.

Figure 7 demonstrates the occurrence distribution binned by the periodicity and the PS angle, similar to Figure 6. The IMF orientations for all and the non-DMI occurring time, as shown in Figures 7a and 7b, mostly present inward  $(-B_\chi)$  and duskward  $(+B_\gamma)$  between 90° and 180° PS angle. On the other hand, the IMF for the DMI intervals frequently present in both  $(-B_\chi, +B_\gamma)$  and  $(+B_\chi, -B_\gamma)$  directions, as in Figure 7c. Those IMF conditions for the DMI time of microinjection could be expected to form quasi-perpendicular shock in the upstream and dusk sector magnetosheath. Moreover, the IMF with inward components  $(+B_\chi)$  were obviously seen during the non-DMI time, while the outward and inward IMF components  $(-B_\gamma)$  were both significant during the DMI time.

### 4. Discussion

Before discussing the statistical results, the speculation about the sources of microinjections and the corresponding solar wind condition are listed, as in Tables 1 and 2. The possible mechanism that Table 1 shows for the

LIOU ET AL. 6 of 11

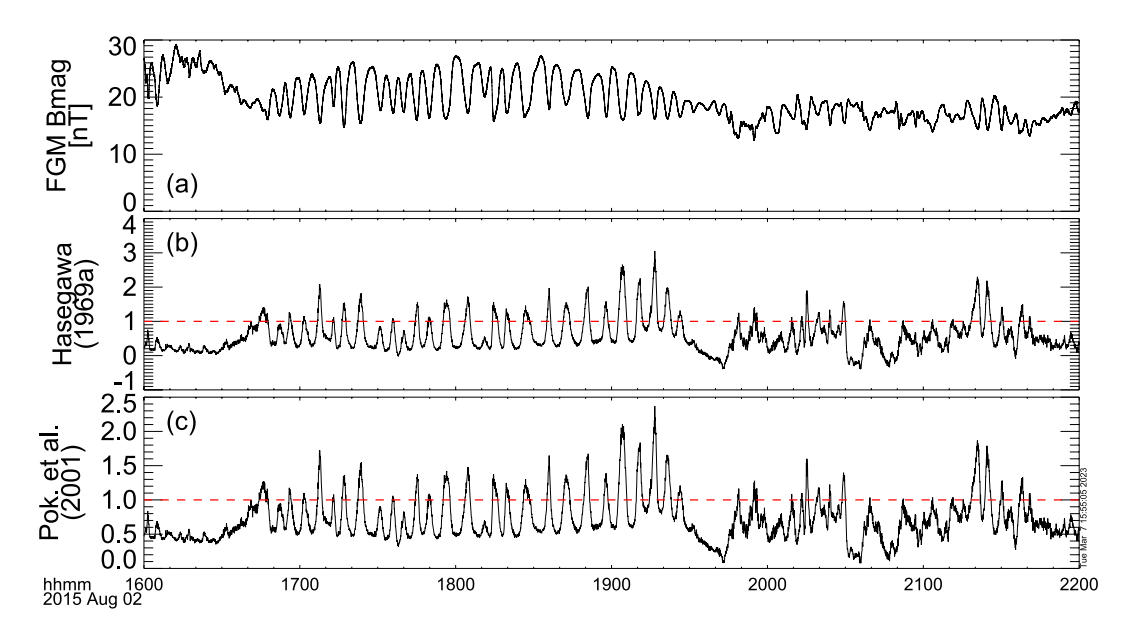
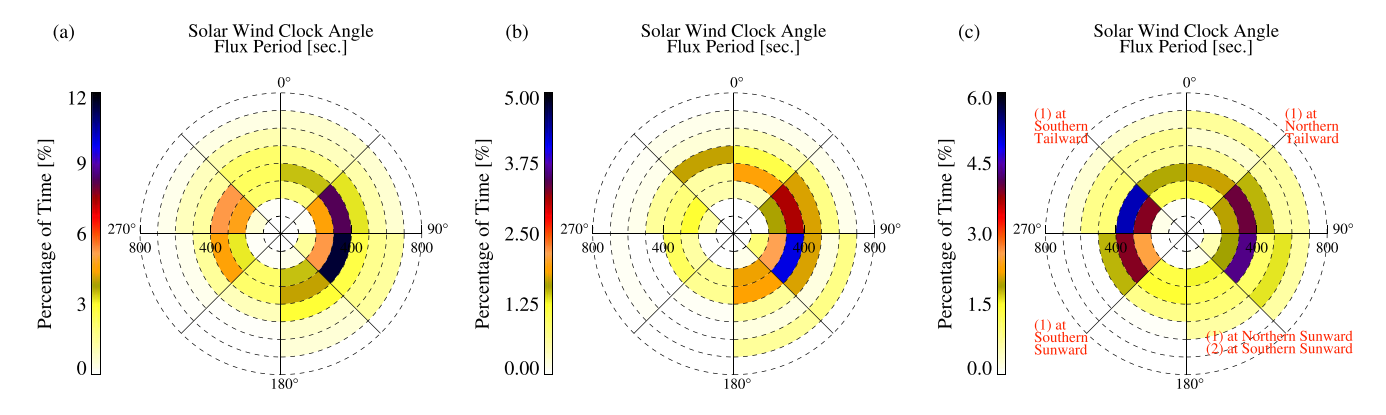


Figure 5. Example of the drift mirror instability criteria. Panel (a) is the magnetic field magnitude, and panels (b, c) are the criteria value calculated respectively with equations from Hasegawa (1969a) and Pokhotelov et al. (2001).

energetic electrons observed at the dusk sector could be the (1) "traditional" DMCs created by high-latitude reconnection (Nykyri, Otto, Adamson, Dougal, & Mumme, 2011), (2) DMCs created by low-latitude component reconnection (Nykyri et al., 2019), (3) the energetic foreshock electrons streaming along the draped IMF, and the (4) radiation belt electrons that get into high-latitude boundary layer by magnetosphere shadowing (Loto'aniu et al., 2010; Turner et al., 2012). In Table 2, the possible sources for the ULF waves could be the (I) drift mirror instability, (II) magnetosheath jet driven compressional surface waves, (III) low-latitude, (IV) high-latitude KHI, (V) FTEs, and (VI) the convected mirror mode waves from downstream of the quasi-perpendicular shock. For better understanding and clearly showing the potential mechanisms for microinjections, the number corresponding to the possible sources listed in Tables 1 and 2 are labeled onto Figures 6 and 7.

The DMCs, formed both at the northern and southern hemisphere by the magnetic reconnection, can locally energize the particles if particles can remain trapped sufficiently long and their drift paths coincide with the reconnection "quasi-potential" (Nykyri et al., 2012). The cavities also provide the temperature anisotropy (Burkholder et al., 2021b; Nykyri et al., 2012) that is responsible for the development of drift mirror instability, which could be the mechanism for the ULF waves. These accelerated particles may leak out from the cavities or be captured and transported by the drift mirror waves or KH waves to their observation site. Considering the



**Figure 6.** The occurrence distribution of electron flux fluctuation periodicity sorted by the interplanetary magnetic field (IMF) clock angle for (a) all occurring time, (b) non-drift mirror instability (DMI) time and (c) DMI time. The radial direction represents the periodicity in units of seconds, while the polar angle represents the IMF clock angle. The 0° direction is the +Z direction in GSM coordinates, while the 90° is the +Y direction. The color code represents the percentage of microinjection occurring time. The red numbers and notes on panel (c) are corresponding to Table 1, describing the possible mechanisms under their favored solar wind condition.

LIOU ET AL. 7 of 11

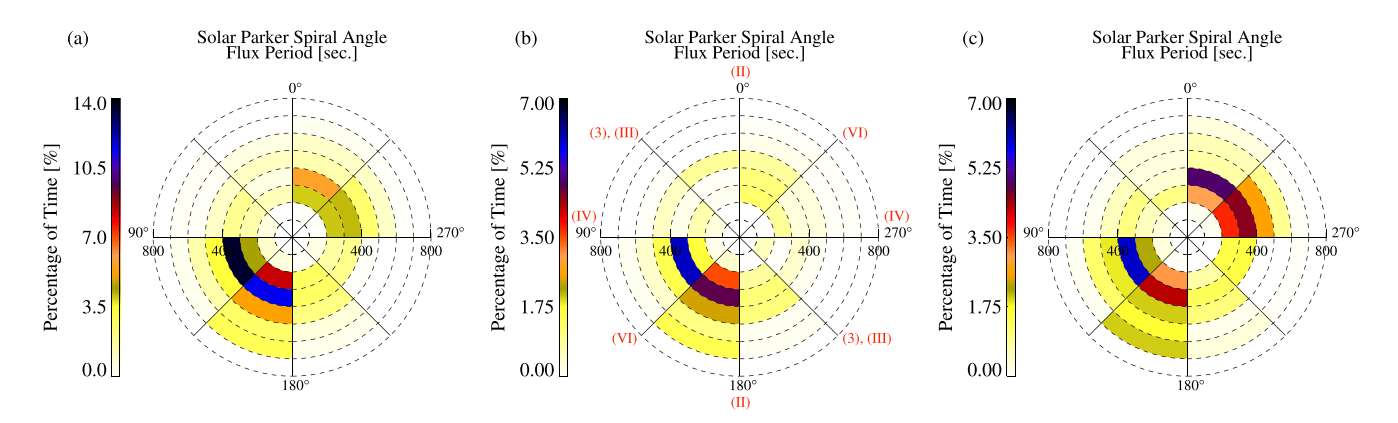


Figure 7. The occurrence distribution of electron flux fluctuation periodicity sorted by the parker spiral angle for (a) all occurring time, (b) non-drift mirror instability (DMI) time and (c) DMI time. The  $0^{\circ}$  direction is pointing to +X, while  $90^{\circ}$  is pointing to +Y in GSM coordinates. The red numbers and notes on panel (b) are corresponding to Table 2, describing the possible ultralow frequency mechanisms under their favored solar wind condition.

location of all of the periodic electron fluxes were observed on the duskside, the possible formation of the DMCs at both north and south hemisphere of dusk sector will be discussed. The energetic particles at the duskside are also expected downstream of the quasi-parallel shock. The particles could be accelerated at the foreshock, where the IMF orientation should be either (a)  $B_X > 0$ ,  $B_Y > 0$  or (b)  $B_X > 0$ ,  $B_Y > 0$ , then streaming along the draped field lines toward the magnetopause. As the quasi-parallel shocks are known to be rippled, the mechanism that generates the wavy structure on the quasi-parallel shocks could also be a candidate for the ULF waves at the inner magnetosphere. For example, a rippled magnetopause surface could be driven by localized high speed magnetosheath jets originating from quasi-parallel shock (Hietala et al., 2009). The KHI and FTEs, as mentioned in the introduction, are also potential candidates for the ULF oscillation seen during microinjections (Kavosi et al., 2018). Statistically, the PS orientation of the IMF mostly forms the quasi-perpendicular shock on the dusk-side magnetosheath. Such an IMF orientation would generate a strong magnetic field tension at the dusk sector magnetopause and thus may stabilize the KH mode (Henry et al., 2017; Nykyri, 2013). This suggests that the low-latitude KHI would favor not only  $B_Z$  dominating but also  $B_X > 0$ ,  $B_Y > 0$  or  $B_X < 0$ ,  $B_Y < 0$  for the duskside flank. One should note that while the IMF orientation is a precondition for the onset of a KHI, it can still be excited for PS orientation at dusk flank if adequate shear flow is present (Henry et al., 2017).

For the DMI microinjections (Figures 6c and 7c), their corresponding IMF exhibits the orientation quasi-perpendicular to the duskside magnetopause. As mentioned earlier, the DMCs are proposed to enable the temperature anisotropy and activate the drift mirror instability at the high latitude (Burkholder et al., 2021a; Nykyri et al., 2012, 2021), the location of these cavities would be crucial when discussing the source of energetic electrons. According to the prevailing IMF orientation during the time of the DMI microinjections, as shown in Figures 6 and 7, we expect to have cavity tailward (sunward) of the cusp funnel for northward (southward) IMF for negative IMF  $B_y$  at the dusk sector southern hemisphere. For the dusk sector northern hemisphere, we expect

 Table 1

 The Possible Sources for the Energetic Particles at the Dusk Sector

		Fav	Favored solar wind condition		
No.	Mechanism	Hemisphere <sup>a</sup>		Sunward <sup>b</sup>	Tailwardc
(1)	Traditional DMCs by high-latitude reconnection	Northern	$B_{\gamma} > 0$	$B_Z < 0$	$B_Z > 0$
		Southern	$B_Y < 0$	$B_Z < 0$	$B_Z > 0$
(2)	DMCs by low-latitude component reconnection	Southern	$B_{\gamma} > 0$	$B_Z < 0$	
(3)	Foreshock particles		$B_X > 0, B_Y > 0$		
			$B_X < 0, B$	$t_{\gamma} < 0$	
(4)	Radiation belt/magnetosphere shadowing	Periodic solar wind dynamic pressure			

<sup>a</sup>The location of DMCs are at the north/south hemisphere. <sup>b</sup>The location of DMCs are at the sunward/tailward side of magnetosphere. <sup>c</sup>Note that the sunward/tailward do not represent the direction of IMF.

LIOU ET AL. 8 of 11



Table 2           The Possible Sources for the Ultralow Frequency Waves at the Dusk Sector					
No.	Mechanism	Favored solar wind condition			
(I)	Drift mirror instability formed nearby the DMCs	Listed in No. (1) and (2) in Table 1			
(II)	Magnetosheaeth jets	$B_X$ dominating			
(III)	Low-latitude	$B_X > 0, B_Y > 0$			
	Kelvin-Helmholtz instability	$B_X < 0, B_Y < 0$			
(IV)	High-latitude Kelvin-Helmholtz instability	$B_{\gamma}$ < 0 for southern hemisphere			
		$B_{\gamma} > 0$ for northern hemisphere			
(V)	Flux transfer events				
(VI)	Convected mirror mode	$B_X > 0, B_Y < 0$			
		$B_X < 0, B_Y > 0$			
(VII)	Radiation belt/magnetosphere shadowing	Periodic solar wind dynamic pressure			

to have cavity tailward (sunward) of the cusp funnel for northward (southward) IMF for positive IMF  $B_{\gamma}$ . Particles inside the cavities at both hemispheres may leak out if magnetic topology is suddenly changed (e.g., via changing IMF). The exact microphysical mechanism of how this happens is still not determined, but may be related to pitch-angle diffusion (Nykyri et al., 2023).

During the microinjection observation times when the DMI condition is not locally satisfied (Figures 6b and 7b), the IMF is mostly inward and duskward, which favors the formation of the quasi-perpendicular shocks at the dusk sector. Since the particle acceleration, ULF fluctuations and high-speed jets mostly occur at foreshock upstream of the quasi-parallel shocks, this orientation of the IMF could be related to fluctuations driven either by low-/high-latitude KHI (if velocity shear is large enough) or magnetosheath mirror mode waves that are convected to the magnetopause and produce compressional fluctuations detected at the MMS location.

A case study in Kavosi et al. (2018) has shown a good agreement between the microinjection signatures and the KHI/FTEs from OpenGGCM. In this global simulation, the period of oscillations at the magnetopause is similar to the period of the observed microinjections. It is likely that the KHI and the FTEs are modulating the magnetospheric boundary, where the high energy particles are preexisting. Although our results do not show clear evidence of a link between KHI and microinjection, they are still possibly compatible. We detected mostly dispersiveness microinjections indicating that MMS was close to the source region, while (Kavosi et al., 2018) detected dispersive microinjections further down the tail, indicating their source region was closer to the Earth, but fluxes were just modulated by the KH waves. On the other hand, a recent statistical survey by Kieokaew et al. (2021) has shown that there is no spatial preference for FTEs for different IMF orientations. The  $B_{\gamma}$  component of the IMF could only determine the helicity of the flux ropes. Hence, Our statistics in the IMF angle would be inadequate to reveal the connection between FTEs and the microinjection. A further study would be required to investigate their relationship.

The magnetopause shadowing is listed both in Tables 1 and 2 since such an expansion and shrinkage could possibly bring the radiation belt energetic particles back and forward and present the signature of microinjections. The periodic oscillations of solar wind dynamic pressure at ULF frequencies observed during microinjections are therefore checked for such shadowing. However, these ULF waves are not seen in the solar wind. Therefore, we doubt that the microinjections are associated with the solar wind dynamic pressure variations for our events.

To summarize, the only mechanisms consistent with the IMF orientation and supporting the ULF generation at the MMS location during the times when local DMI condition is not met are the convected magnetosheath mirror mode waves downstream from the quasi-perpendicular shock and KH waves. The convected mirror mode waves could produce compressional fluctuations at the magnetopause which are observed by the MMS and where a local DMI criteria is no longer fulfilled. However, the asymmetric patterns showing in Figures 6b and 7b are still inexplicable since the outward, dawnward solar wind can also form the quasi-perpendicular shocks upstream and trigger the mirror mode. This asymmetry may hint at the other sources, for example, magnetic reconnection driven FTEs for different dipole tilt angles. The enhanced tailward dipole tilt together with inward IMF would

LIOU ET AL. 9 of 11



produce a higher magnetic shear at the southern hemispheric dayside magnetosphere, making it more prone to reconnection and FTEs.

#### 5. Conclusions

In this study, we have presented results of the statistical investigation of the counter-streaming energetic electron microinjections. We have performed an overall search of MMS boundary layer crossing from 2015 to 2017. These clear events are found only existing on the dusk side and mostly, at the southern high-latitude sector of magnetosphere. The investigation for the drift mirror mode shows 62% of total microinjection time satisfying the instability criteria, which emphasizes the importance of the DMI responsible for the microinjection activity. Both northern and southern hemispheric DMCs are expected to provide energetic electrons and generate ion temperature anisotropy to create DMI and microinjection signatures.

For the non-DMI microinjection events, the IMF were favoring the duskward and earthward orientation (but not the dawnward and sunward orientation), which favors quasi-perpendicular shock generation upstream of the duskside magnetosphere. Under such the IMF condition, the possible mechanism is the mirror mode waves propagated from downstream of the quasi-perpendicular shocks to the magnetopause. However, this converted mirror mode can only explain the appearance of ULF waves at the inner magnetosphere. Also, the asymmetry (lack of observations for dawnward and sunward IMF) is puzzling.

The possible sources of the energetic particles such as the foreshock acceleration or radiation belt shadowing are not consistent with the observed IMF and solar wind dynamic pressure variations. Thus, a connection between the source of energetic electrons and the periodic property during the non locally DMI driven microinjection events should be further studied in the future when simultaneous spacecraft measurements become available close to the shock, magnetosheath and close to magnetopause. The possible MMS string-of-pearls configuration with larger spacecraft separation, or conjunctions with THEMIS would be ideal to solve this puzzle.

# **Data Availability Statement**

We are grateful for the entire MMS mission team leads for data access. The MMS data were downloaded through the MMS Science Data Center (https://lasp.colorado.edu/mms/sdc/public/). The versions of the data files used are v4.18.0.cdf, v5.87.0.cdf, v5.100.0, v5.104, v5.105.0.0, v5.108.0, v5.109.0, and v5.112.0.cdf for FGM survey mode; v3.3.0.cdf for FPI fast mode, v6.1.2.cdf and v7.1.1.cdf for FEEPS survey mode respectively. We acknowledge use of NASA/GSFC's Space Physics Data Facility's CDAWeb service (https://cdaweb.gsfc.nasa.gov/), and OMNI data. We also acknowledge the SPEDAS software used for the analysis (Angelopoulos et al., 2019). The figure data used in the paper are available in Liou and Nykyri (2023).

#### ${\bf Acknowledgments}$

Support for this research was provided by NASA Grants 80NSSC18K1381 and 80NSSC22K0304 to the Embry-Riddle Aeronautical University. This research was also based upon work supported by the NSF award under #2308853. In addition work by Yu-Lun Liou and Katariina Nykyri was supported by the International Space Science Institute (ISSI) in Bern, through ISSI International Team Project #546 "Magnetohydrodynamic Surface Waves at Earth's Magnetosphere (and Bevond)."

#### References

Angelopoulos, V., Cruce, P., Drozdov, A., Grimes, E., Hatzigeorgiu, N., King, D., et al. (2019). The space physics environment data analysis system (SPEDAS). Space Science Reviews, 215(1), 9. https://doi.org/10.1007/s11214-018-0576-4

Arnoldy, R. L., & Chan, K. W. (1969). Particle substorms observed at the geostationary orbit. *Journal of Geophysical Research*, 74(21), 5019–5028. https://doi.org/10.1029/JA074i021p05019

Burkholder, B. L., Nykyri, K., & Ma, X. (2021a). Magnetospheric multiscale statistics of high energy electrons trapped in diamagnetic cavities. Journal of Geophysical Research: Space Physics, 126(1), e2020JA028341. https://doi.org/10.1029/2020JA028341

Burkholder, B. L., Nykyri, K., Ma, X., Sorathia, K., Michael, A., Otto, A., & Merkin, V. (2021b). The structure of the cusp diamagnetic cavity and test particle energization in the GAMERA global MHD simulation. *Journal of Geophysical Research: Space Physics*, 126(12), e2021JA029738. https://doi.org/10.1029/2021JA029738

Chen, J. S., & Fritz, T. A. (1998). Correlation of cusp MeV helium with turbulent ULF power spectra and its implications. *Geophysical Research Letters*, 25(22), 4113–4116. https://doi.org/10.1029/1998GL900122

Czaykowska, A., Bauer, T. M., Treumann, R. A., & Baumjohann, W. (1998). Mirror waves downstream of the quasi-perpendicular bow shock. Journal of Geophysical Research, 103(A3), 4747–4753. https://doi.org/10.1029/97JA03245

Czaykowska, A., Bauer, T. M., Treumann, R. A., & Baumjohann, W. (2001). Magnetic field fluctuations across the Earth's bow shock. *Annales Geophysicae*, 19(3), 275–287. https://doi.org/10.5194/angeo-19-275-2001

Fennell, J. F., Turner, D. L., Lemon, C. L., Blake, J. B., Clemmons, J. H., Mauk, B. H., et al. (2016). Microinjections observed by mms FEEPS in the dusk to midnight region. *Geophysical Research Letters*, 43(12), 6078–6086. https://doi.org/10.1002/2016GL069207

Haerendel, G. (2000). Outstanding issues in understanding the dynamics of the inner plasma sheet and ring current during storms and substorms. Advances in Space Research, 25(12), 2379–2388. https://doi.org/10.1016/S0273-1177(99)00527-X

Hasegawa, A. (1969a). Drift mirror instability in the magnetosphere. *The Physics of Fluids*, 12(12), 2642–2650. https://doi.org/10.1063/1.1692407 Hasegawa, A. (1969b). Heating of the magnetospheric plasma by electromagnetic waves generated in the magnetosheath. *Journal of Geophysical Research*, 74(7), 1763–1771. https://doi.org/10.1029/JA074i007p01763

LIOU ET AL. 10 of 11



- Henry, Z. W., Nykyri, K., Moore, T. W., Dimmock, A. P., & Ma, X. (2017). On the dawn-dusk asymmetry of the Kelvin-Helmholtz instability between 2007 and 2013. *Journal of Geophysical Research: Space Physics*, 122(12), 11888–11900. https://doi.org/10.1002/2017JA024548
- Hietala, H., Laitinen, T. V., Andréeová, K., Vainio, R., Vaivads, A., Palmroth, M., et al. (2009). Supermagnetosonic jets behind a collisionless quasiparallel shock. *Physical Review Letters*, 103(24), 245001. https://doi.org/10.1103/PhysRevLett.103.245001
- Hubert, D., Perche, C., Harvey, C. C., Lacombe, C., & Russell, C. T. (1989). Observation of mirror waves downstream of a quasi-perpendicular shock. Geophysical Research Letters, 16(2), 159–162. https://doi.org/10.1029/GL016i002p00159
- Kavosi, S., Spence, H. E., Fennell, J. F., Turner, D. L., Connor, H. K., & Raeder, J. (2018). MMS/FEEPS observations of electron microinjections due to Kelvin-Helmholtz waves and flux transfer events: A case study. *Journal of Geophysical Research: Space Physics*, 123(7), 5364–5378. https://doi.org/10.1029/2018JA025244
- Kieokaew, R., Lavraud, B., Fargette, N., Marchaudon, A., Génot, V., Jacquey, C., et al. (2021). Statistical relationship between interplanetary magnetic field conditions and the helicity sign of flux transfer event flux ropes. Geophysical Research Letters, 48(6), e2020GL091257. https://doi.org/10.1029/2020GL091257
- King, J. H., & Papitashvili, N. E. (2005). Solar wind spatial scales in and comparisons of hourly wind and ACE plasma and magnetic field data. Journal of Geophysical Research, 110, 2104. https://doi.org/10.1029/2004JA010649
- Lacombe, C., Pantellini, F. G. E., Hubert, D., Harvey, C. C., Mangeney, A., Belmont, G., & Russell, C. T. (1992). Mirror and Alfvenic waves observed by ISEE 1-2 during crossings of the Earth's bow shock. *Annales Geophysicae*, 10(10), 772–784.
- Liou, Y.-L., & Nykyri, K. (2023). Statistical study of the energetic electron microinjections at the high-latitude magnetosphere [Figure]. https://doi.org/10.6084/m9.figshare.23979381.v2
- Loto'aniu, T. M., Singer, H. J., Waters, C. L., Angelopoulos, V., Mann, I. R., Elkington, S. R., & Bonnell, J. W. (2010). Relativistic electron loss due to ultralow frequency waves and enhanced outward radial diffusion. *Journal of Geophysical Research*, 115(A12), A12245. https://doi.org/10.1029/2010JA015755
- Mauk, B. H., Blake, J. B., Baker, D. N., Clemmons, J. H., Reeves, G. D., Spence, H. E., et al. (2016). The energetic particle detector (EPD) investigation and the energetic ion spectrometer (EIS) for the magnetospheric multiscale (MMS) mission. Space Science Reviews, 199(1–4), 471–514. https://doi.org/10.1007/s11214-014-0055-5
- Niehof, J. T., Fritz, T. A., Friedel, R. H. W., & Chen, J. (2008). Interdependence of magnetic field and plasma pressures in cusp diamagnetic cavities. *Geophysical Research Letters*, 35(11), L11101. https://doi.org/10.1029/2008g1033589
- Nykyri, K. (2013). Impact of MHD shock physics on magnetosheath asymmetry and Kelvin-Helmholtz instability. *Journal of Geophysical Research: Space Physics*, 118(8), 5068–5081. https://doi.org/10.1002/jgra.50499
- Nykyri, K., Cargill, P. J., Lucek, E., Horbury, T. S., Balogh, A., Lavraud, B., et al. (2003). Ion cyclotron waves in the high altitude cusp: Cluster observations at varying spacecraft separations. Geophysical Research Letters, 30(24), 2263–2269. https://doi.org/10.1029/2003GL018594
- Nykyri, K., Cargill, P. J., Lucek, E. A., Horbury, T. S., Lavraud, B., Balogh, A., et al. (2004). Cluster observations of magnetic field fluctuations in the high-altitude cusp. *Annales Geophysicae*, 22(7), 2413–2429. https://doi.org/10.5194/angeo-22-2413-2004
- Nykyri, K., Chu, C., Ma, X., Fuselier, S. A., & Rice, R. (2019). First MMS observation of energetic particles trapped in high-latitude magnetic field depressions. *Journal of Geophysical Research: Space Physics*, 124(1), 197–210. https://doi.org/10.1029/2018JA026131
- Nykyri, K., Johnson, J., Kronberg, E., Turner, D., Wing, S., Cohen, I., et al. (2021). Magnetospheric multiscale observations of the source region of energetic electron microinjections along the duskside, high-latitude magnetopause boundary layer. Geophysical Research Letters, 48(9), e2021GL092466. https://doi.org/10.1029/2021GL092466
- Nykyri, K., Liou, Y., Ma, X., Kavosi, S., Egedal, J., Fuselier, S. A., & Gomez, R. G. (2023). Wave analysis during energetic electron microinjections: A case study. *Physics of Plasmas*, 30(7), 072903. https://doi.org/10.1063/5.0142938
- Nykyri, K., Otto, A., Adamson, E., Dougal, E., & Mumme, J. (2011). Cluster observations of a cusp diamagnetic cavity: Structure, size, and dynamics. *Journal of Geophysical Research*, 116(A3), 3228. https://doi.org/10.1029/2010JA015897
- Nykyri, K., Otto, A., Adamson, E., Kronberg, E., & Daly, P. (2012). On the origin of high-energy particles in the cusp diamagnetic cavity. *Journal of Atmospheric and Solar-Terrestrial Physics*, 87, 70–81. https://doi.org/10.1016/j.jastp.2011.08.012
- Nykyri, K., Otto, A., Adamson, E., & Tjulin, A. (2011). On the origin of fluctuations in the cusp diamagnetic cavity. *Journal of Geophysical Research*, 116(A6), 6208. https://doi.org/10.1029/2010JA015888
- Pokhotelov, O. A., Balikhin, M. A., Treumann, R. A., & Pavlenko, V. P. (2001). Drift mirror instability revisited, 1, cold electron temperature limit. *Journal of Geophysical Research*, 106(A5), 8455–8463. https://doi.org/10.1029/2000JA000069
- Pollock, C., Moore, T., Jacques, A., Burch, J., Gliese, U., Saito, Y., et al. (2016). Fast plasma investigation for magnetospheric multiscale. Space
- Science Reviews, 199(1-4), 331-406. https://doi.org/10.1007/s11214-016-0245-4
  Russell, C. T., Anderson, B. J., Baumjohann, W., Bromund, K. R., Dearborn, D., Fischer, D., et al. (2016). The magnetospheric multiscale

magnetometers, Space Science Reviews, 199(1-4), 189-256, https://doi.org/10.1007/s11214-014-0057-3

- Sarafopoulos, D. V. (2002). Dispersive and repetitive Pc5 mode microinjections in the inner magnetosphere. Geophysical Research Letters, 29(8), 26-1–26-4. https://doi.org/10.1029/2001GL014067
- Shue, J.-H., Chao, J. K., Fu, H. C., Russell, C. T., Song, P., Khurana, K. K., & Singer, H. J. (1997). A new functional form to study the solar wind control of the magnetopause size and shape. *Journal of Geophysical Research*, 102(A5), 9497–9511. https://doi.org/10.1029/97JA00196
   Torbert, R. B., Vaith, H., Granoff, M., Widholm, M., Gaidos, J. A., Briggs, B. H., et al. (2016). The electron drift instrument for MMS. *Space*
- Science Reviews, 199(1–4), 283–305. https://doi.org/10.1007/s11214-015-0182-7

  Treumann, R. A., Jaroschek, C. H., Constantinescu, O. D., Nakamura, R., Pokhotelov, O. A., & Georgescu, E. (2004). The strange physics of low frequency mirror mode turbulence in the high temperature plasma of the magnetosheath. Nonlinear Processes in Geophysics, 11(5/6),
- 647–657. https://doi.org/10.5194/npg-11-647-2004

  Tsurutani, B. T., Smith, E. J., Anderson, R. R., Ogilvie, K. W., Scudder, J. D., Baker, D. N., & Bame, S. J. (1982). Lion roars and nonoscillatory drift mirror waves in the magnetosheath. *Journal of Geophysical Research*, 87(A8), 6060–6072. https://doi.org/10.1029/JA087iA08p06060
- Turner, D. L., Fennell, J. F., Blake, J. B., Claudepierre, S. G., Clemmons, J. H., Jaynes, A. N., et al. (2017). Multipoint observations of energetic particle injections and substorm activity during a conjunction between magnetospheric multiscale (MMS) and Van Allen probes. *Journal of Geophysical Research: Space Physics*, 122(11), 11481–11504. https://doi.org/10.1002/2017JA024554
- Turner, D. L., Shprits, Y., Hartinger, M., & Angelopoulos, V. (2012). Explaining sudden losses of outer radiation belt electrons during geomagnetic storms. *Nature Physics*, 8(3), 208–212. https://doi.org/10.1038/nphys2185
- Walsh, B. M., Fritz, T. A., Klida, M. M., & Chen, J. (2010). Energetic electrons in the exterior cusp: Identifying the source. *Annales Geophysicae*, 28(4), 983–992. https://doi.org/10.5194/angeo-28-983-2010
- Woch, J., Kremser, G., Korth, A., Pokhotelov, O., Pilipenko, V., Nezlina, Y., & Amata, E. (1988). Curvature-driven drift mirror instability in the magnetosphere. *Planetary and Space Science*, 36(4), 383–393. https://doi.org/10.1016/0032-0633(88)90126-2

LIOU ET AL.